

Dynamic impact behavior of syntactic foam core sandwich composites

P Breunig¹, V Damodaran¹, K Shahapurkar², S Waddar³ ,
M Doddamani³, P Jeyaraj³  and P Prabhakar¹ 

Abstract

Sandwich composites and syntactic foams independently have been used in many engineering applications. However, there has been minimal effort towards taking advantage of the weight saving ability of syntactic foams in the cores of sandwich composites, especially with respect to the impact response of structures. To that end, the goal of this study is to investigate the mechanical response and damage mechanisms associated with syntactic foam core sandwich composites subjected to dynamic impact loading. In particular, this study investigates the influence of varying cenosphere volume fraction in syntactic foam core sandwich composites subjected to varying dynamic impact loading and further elucidates the extent and diversity of corresponding damage mechanisms. The syntactic foam cores are first fabricated using epoxy resin as the matrix and cenospheres as the reinforcement with four cenosphere volume fractions of 0% (pure epoxy), 20%, 40%, and 60%. The sandwich composite panels are then manufactured using the vacuum assisted resin transfer molding process with carbon fiber/vinyl ester facesheets. Dynamic impact tests are performed on the sandwich composite specimens at two energy levels of 80 J and 160 J, upon which the data are post-processed to gain a quantitative understanding of the impact response and damage mechanisms incurred by the specimens. A qualitative understanding is obtained through micro-computed tomography scanning of the impacted specimens. In addition, a finite element model is developed to investigate the causes for different damage mechanisms observed in specimens with different volume fractions.

Keywords

Syntactic foam, sandwich composites, dynamic impact, vacuum assisted resin transfer molding, cenospheres

Introduction

Composite materials typically allow for structural properties to be optimized such that the strength and weight constraints are more easily met in the design of everyday structures. This is evident as composites continue to become more prevalent in aerospace, naval, and civil applications.¹ Sandwich composites typically consist of two stiff outer facesheets (away from the natural axis) usually made of fiber-reinforced polymer that sandwich a lightweight core between them. This provides stiffness to the cross-section and resists majority of the bending stresses. The lightweight core connects the two facesheets and assists with shear transfer in the section.

A large body of research has been conducted by previous researchers to better understand the behavior of sandwich composites using different materials and loading conditions. A few notable works reported on the low-velocity impact behavior of foam core

sandwich composites include, but are not limited to Daniel et al.,² Schubel et al.,³ Zhang et al.,⁴ Wang et al.,⁵ Nemes and Simmonds,⁶ Mines et al.,⁷ Erickson et al.,⁸ Salehi-Khojin et al.,⁹ Yang et al.,¹⁰ and Tan et al.¹¹ Schubel et al. investigated the low-velocity impact behavior of polyvinyl chloride foam cores with woven carbon fiber/epoxy facesheets and compared the performance to quasi-static tests for the same materials.³ The results showed that the damage observed in the low-velocity impact tests was comparable to the damage in quasi-static tests at the same

¹University of Wisconsin-Madison, USA

²Sanjeevan Engineering and Technology Institute, India

³National Institute of Technology, Karnataka, India

Corresponding author:

P Prabhakar, Engineering Hall Room 2210, University of Wisconsin-Madison, 1415 Engineering Drive Madison, WI 53706, USA.
Email: pavana.prabhakar@wisc.edu

compressive strain level. Work by Hazizan and Cantwell¹² reported the low-velocity impact response of sandwich structures with foam cores and glass fiber-reinforced facesheets. Results showed that for a specific impact energy, the maximum recorded force increased as the shear modulus of the core increased. The failure mechanism transitioned from shear cracks in the core to delamination between the core and facesheet as the density of the core increased. Elamin et al.¹³ evaluated the damage of sandwich structures under dynamic impact loading, which were exposed to arctic conditions with temperatures ranging from 23°C to -70°C. PVC foam cores were used with facesheets of 0°/90° woven carbon fiber-reinforced laminate with epoxy matrix. The article concluded that the peak impact force recorded decreased as the in-situ test temperature decreased. Also, using micro-computed tomography (micro-CT), the authors noted that the specimens experienced higher degree of damage at low temperatures as compared to higher temperatures.

Syntactic foams are closed cell composite foams with hollow micro-spheres dispersed in a matrix resin. The closed cell structure provides excellent mechanical properties, like high strength and low density, in addition to lower moisture absorption as compared to open cell foams.¹⁴ Hence, syntactic foam cores in sandwich composites ensure high rigidity and strength of the sandwich structures as compared to other polymeric foam cores.¹⁴⁻¹⁹ Few widely known applications of syntactic foams are in components for boat decks, ribs, hulls, and floatation modules for offshore structures.²⁰ In addition, they are also used in deep sea applications like remote operated vehicles, submarines, and underwater pipelines. Few potential applications of syntactic foam core sandwich composites could be in building facades, bridge decks, and other civil infrastructure.

In the current study, syntactic foams are used as the core material in sandwich composites. Specifically, cenospheres (fly ash particles) are used as the hollow micro-spheres in these syntactic foams. Past researchers have investigated the behavior of syntactic foams with engineering glass (Sodalime-borosilicate) micro-balloons as the filler material.²¹⁻²³ However, dealkalization of glass has been shown to degrade such syntactic foams.²⁴ Fly ash being a byproduct of coal plants primarily consists of alumina and silica. Hence, use of cenospheres in syntactic foams can aid in minimizing waste from the environment, while creating syntactic foams with better properties as shown by previous researchers.²⁵⁻³⁰

Extensive studies on the mechanical behavior of syntactic foams have been performed by previous researchers exploring their suitability for a wide range of applications^{21,31-33} In the work by Gupta et al.,³⁴ it was shown that the compressive strength and modulus

of syntactic foams increased as the internal radius of cenospheres was reduced, while holding all other parameters fixed. Different types of tests have been performed on syntactic foams, such as three-point bending tests in flexure³⁵⁻³⁷ and short beam shear tests³⁸⁻⁴⁰ to determine their response under such types of loading. Previous works by Garcia et al.⁴¹ and Shahapurkar et al.⁴² investigated the behavior of cenosphere-reinforced syntactic foams in compression and flexure over a range of temperatures. In Garcia et al.,⁴¹ it was observed that the flexural modulus of cenosphere/epoxy syntactic foams increased and the flexural strength decreased with cenosphere volume fraction. Additional analysis showed that the failure strains decreased as the cenosphere volume fraction increased.

Although syntactic foams have not been explored as the core material for sandwich composites under impact loading, they have been studied when subjected to quasi-static loading. Work by Gupta and Woldesenbet⁴³ investigated the flexural properties of sandwich composites with syntactic foam cores. It was reported that the effect of micro-balloon wall thickness to diameter ratio had little effect on the strength of the specimens under three-point bend tests as the failure mechanism was tensile tearing of the facesheets. However, high shear stresses in short beams shear tests resulted in shear cracks within the syntactic foams.

The present study expands on the knowledge of sandwich composites and syntactic foams by using cenosphere/epoxy syntactic foams as the core of sandwich composites and evaluates their dynamic impact response. The sandwich composites are tested under low-velocity impact loading to investigate their dynamic impact response, as well as identify key failure mechanisms and elucidate the reasons for the observed behaviors. The purpose of this study is to gain an understanding of the influence of cenosphere volume fraction in syntactic foams on the impact behavior of the sandwich composites subjected to different impact energies.

Methods and materials

Constituent materials

Sandwich composites in this experimental study consisted of three major constituent materials: a syntactic foam core, woven carbon fiber facesheets, and vinyl ester resin. The syntactic foam core was comprised of cenospheres and Lapox L-12 epoxy resin with K-6 hardener. The cenospheres are hollow particles which are a byproduct of coal production. Each facesheet consisted of four layers of 3K plain weave carbon fiber procured from Fibre Glast Developments Corp. and was cut to fit the dimensions of the core. Each facesheet layer had identical orientation and stacking

of $[(0/90)_{w4}/\text{core}/[(0/90)_{w4}]$. Here, the subscript “w” represents woven carbon fiber layers. Commercially available vinyl ester resin and Methyl Ethyl Ketone Peroxide (MEKP), both procured from Fibre Glast Developments Corp., were used as the matrix in the facesheets.

Manufacturing

Foam core. The syntactic foam cores were fabricated by mixing a weight fraction (equivalent to 20, 40, and 60 volume %) of cenospheres with Lapox L-12 epoxy resin and K-6 hardener at room temperature. A homogeneous and uniform slurry was assured by gentle stirring. Further, 10% by weight hardener was added to the slurry, followed by degassing the mixture for 4 min prior to pouring into aluminum molds. Curing of cast slabs was conducted at room temperature for 24 h and subsequently post cured for 3 h. Different compositions of foam samples were fabricated by varying the cenosphere volume fraction. Specimens with 0% (pure epoxy), 20%, 40%, and 60% cenosphere volume fraction were prepared for use in sandwich composites. Distribution of cenospheres in the syntactic foam core is shown via micro-CT scan in Figure 1.

The weight fractions of the constituent materials (epoxy and cenospheres) for known volume fractions were calculated using the formulas given in equation (1)

$$W_f = \frac{\frac{\rho_f}{\rho_m}}{\frac{\rho_f}{\rho_m} V_f + V_m} V_f; \quad W_m = \frac{1}{\frac{\rho_f}{\rho_m} V_f + V_m} V_m \quad (1)$$

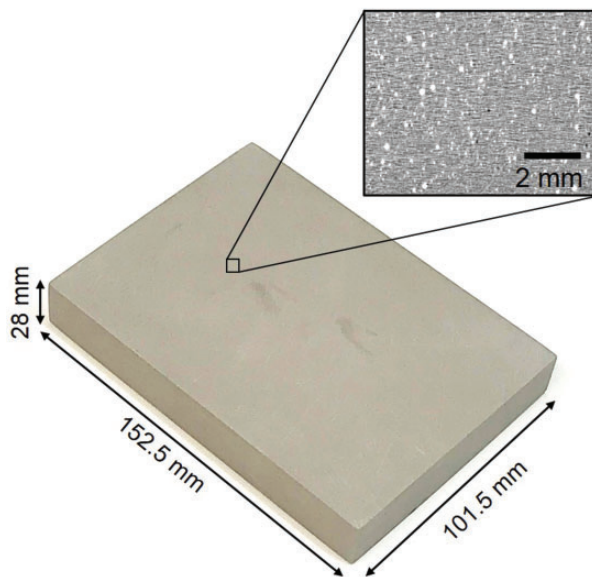


Figure 1. Manufactured cenosphere/epoxy syntactic foam core. Inset shows micro-CT image of internal distribution of cenospheres in epoxy matrix.

where W represents weight fraction, V represents volume fraction, ρ represents density, and the subscripts f and m represent filler and matrix, respectively. The densities of epoxy and cenosphere particles are considered to be 1192 kg/m^3 and 920 kg/m^3 based on measurements previously conducted by Bharath Kumar et al.²⁸, Garcia et al.⁴¹ and Shahapurkar et al.⁴² Based on the dimensions of a mold, the volume of composite (V_c) to be prepared was found. The weights of cenospheres and epoxy for known volume fractions were calculated using the values of weight fraction.

Sandwich composite. The sandwich composites were manufactured with the vacuum assisted resin transfer molding (VARTM) process. The VARTM process was conducted on a flat aluminum mold plate. Vacuum was created between the mold plate, vacuum sealant tape, and vacuum bag (Stretchlon 800 Bagging Film) using two vacuum pumps (60–80 MPa vacuum pressure). One hundred parts of vinyl ester resin were mixed with 1.25 parts of MEKP by mass as per the manufacturer’s instructions. The first pump was used to infuse this resin mixture through the specimen and was removed once the infusion process was complete (5 min in duration). This pump corresponded to an inner vacuum bag. The outer vacuum bag applied pressure during the resin curing process which lasted for 3 h from the time the vinyl ester was initially mixed. The specimens were cured for at least 24 h after resin infusion, after which they were removed from the mold.

Several best practices were employed to ensure the fabrication of high-quality sandwich composites. First, a combination of HDPE Infusion Flow Media, cotton breather, and 1586 PTFE-Coated FG (all procured from Fibre Glast Developments Corp.) were used in addition to the carbon fiber to ensure a consistent distribution of vinyl ester resin and allow for easy removal of the specimens from the mold upon curing. Second, the vinyl ester resin mixture was degassed prior to the infusion to help prevent voids forming in the facesheets. The degassing continued until air bubbles in the resin were no longer visually detectable in the resin. Finally, resin dams were constructed to direct the flow of resin through the facesheets and not just around the specimens. Due to the relatively low viscosity of vinyl ester resin and large thickness of the sandwich composite, the vinyl ester resin was susceptible to flow around the specimen forming many unwanted voids and poor bonding between the core and facesheets. The dams consisted of extra vacuum tape applied to the sides of the specimen perpendicular to the direction of resin flow. A schematic of the manufacturing process is shown in Figure 2.

The dimensions of the manufactured sandwich composites were 175 mm long by 125 mm wide, from which

the samples were water jet cut to nominal values of 150 mm × 100 mm rectangles as per the ASTM D7766⁴⁴ standard. The actual average dimensions of the tested specimens were 152.5 mm × 101.5 mm × 28.0 mm with standard deviations of 0.2 mm, 0.3 mm, and 0.3 mm, respectively. The densities of these samples were measured and are summarized in Table 1. These densities were measured after manufacturing the sandwich composite, which allowed for comparison of the in-service state rather than determining those of just the cores. The densities of the specimens decreased as the cenosphere volume fraction increased.

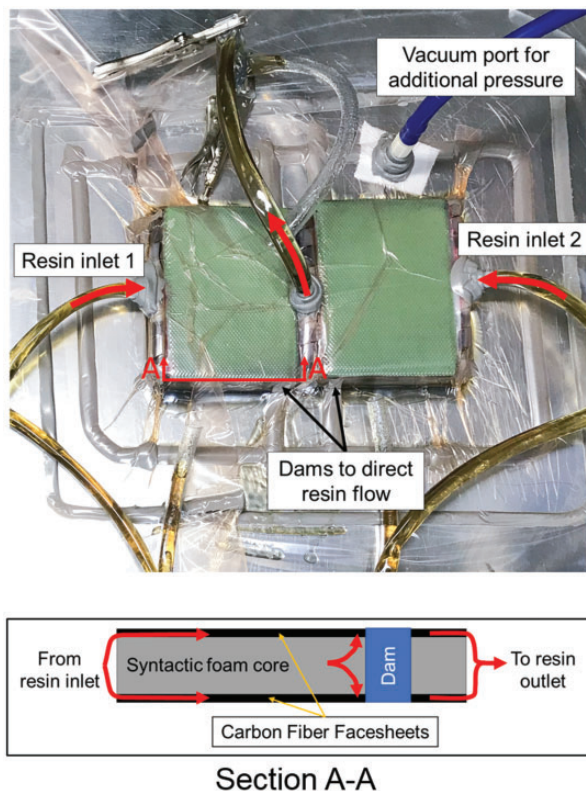


Figure 2. Vacuum assisted resin transfer molding (VARTM) process during the sandwich fabrication stage. Section A-A depicts the front face of the sandwich, which shows flow of resin in front of the core. The dams assist in diverting the resin to flow through the carbon fiber facesheets. The red arrows depict the flow path of the resin.

Dynamic impact testing

The sandwich composite specimens were tested under dynamic impact (ASTM D7766)⁴⁴ at two different energy levels corresponding to 80 J and 160 J. These two energy levels were determined via a preliminary testing program of the manufactured sandwich composites. They were chosen due to distinct failure mechanisms observed at the two energy levels. In total, 24 sandwich composite specimens were tested with 12 at each energy level. Of the 12 specimens at each energy level, 4 different volume fractions of cenospheres in the core were used yielding 3 specimens for each test case.

Drop-weight impact tests were performed using a CEAST 9350 Accelerated Drop Tower Impact System fitted with a hemispherical striker at the University of Wisconsin—Madison. The clamped boundary conditions shown in Figure 3 are consistent with ASTM D7766.⁴⁴ Force, displacement, energy versus time responses were recorded by the data acquisition system “CEAST DAS 8000 Junior” for each test at a sampling rate of 500 kHz. A 5 m/s impact velocity, well within the range of low velocity impact, was chosen for the tests to ensure uniform propagation behavior between the striker and specimen at different energy levels. To achieve this constant impact velocity, additional mass was added to the striker in order to attain impact energy of 160 J. In all, 6.5 kg of total mass was used for the 80 J tests, while 12.5 kg was

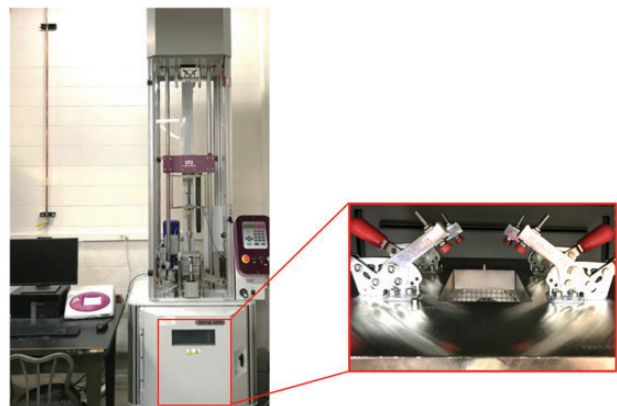


Figure 3. CEAST 9350 Impact Machine with anti-rebound mechanism and testing chamber (inset) with fixture to simulate clamped boundary conditions consistent with ASTM D7766.

Table 1. Summary of manufactured density of sandwich composite specimens.

Cenosphere volume fraction	0%	20%	40%	60%
Average (kg/m ³)	1314 ± 3	1220 ± 12	1147 ± 17	1095 ± 17
Change (%)	0	−7.1	−12.7	−16.7

used for the 160J tests. The impact testing machine's anti-rebound mechanism was activated to avoid multiple impacts on the sample.

Finite element model description

A finite element (FE) analysis was performed to understand the micro-mechanical material response of the syntactic foam at different cenosphere volume fractions. The indentation of the steel striker onto the syntactic foam was modeled as a quasi-static loading rather than an impact analysis to obtain a qualitative understanding of the strain distribution. Strain rate effects were ignored in the epoxy as the goal of this analysis was to obtain a qualitative understanding of the strain distribution in the syntactic foam core underneath the striker location. With the output from the FE model, strain contours were analyzed and compared with failure mechanisms observed in the micro-CT scans to help explain the possible causes for damage mechanisms at certain volume fractions.

The FE model was divided into two subregions as shown in Figure 4. A finely meshed two-phase region with the epoxy matrix and hollow spherical cenosphere inclusions directly under the impact location, and a larger homogenized media (shown in green in Figure 4) with coarser mesh away from the impact location. The purpose of the two subregions was to simulate a larger syntactic foam domain while

capturing the details of the behavior in the vicinity of the impact location and including the effects of boundary conditions away from the impact location. A symmetric boundary condition was considered about the axis of the striker, which was introduced as a restriction in the horizontal translation on the left face of the domain as shown in Figure 4. Further, contact conditions between the syntactic foam core and the steel striker at the top, and the support at the bottom ensured more realistic boundary conditions. To reduce the complexity of the FE model, carbon fiber face sheets were not modeled as the goal of this simulation was to investigate the damage patterns in the foam core.

Material properties for the homogenized core and the epoxy matrix were obtained from recent work by Shahapurkar et al.⁴² where the authors investigated the compressive modulus and strength of cenosphere/epoxy syntactic foam cores. The average compressive elastic modulus values from Shahapurkar et al.⁴² were used for the homogenized region of the FE model. Using a rule of mixtures approach, the average compressive modulus of the cenospheres was calculated. In this calculation, the cenospheres were idealized as hollow spherical particles with a constant wall thickness of 5 μm and a mean diameter of 110 μm ⁴² to back-calculate the equivalent elastic modulus of the cenospheres which was found to be 40 GPa. The input values for the modulus are summarized in Table 2.

To account for the crushing of syntactic foam cores, the cenosphere, epoxy matrix, and homogenized region were modeled as elastic-perfectly plastic materials. The matrix in the two-phase region was modeled to yield at 104.8 MPa, which is a mean value of the compressive strength reported by Shahapurkar et al.⁴² for the 0% cenosphere volume fraction. Similarly, the homogenized media was modeled to yield at the mean values reported for the respective volume fractions of 20%, 40% and 60%. The cenospheres were modeled to crush at a stress value vastly different from that of the matrix to help differentiate the materials in the output strain field. An assumed yield stress of 150 MPa was chosen. A verification analysis showed that both higher and lower assumed yield stress values for cenospheres as compared to that of matrix strength produced similar strain patterns, which help with qualitatively explaining the crack propagation.

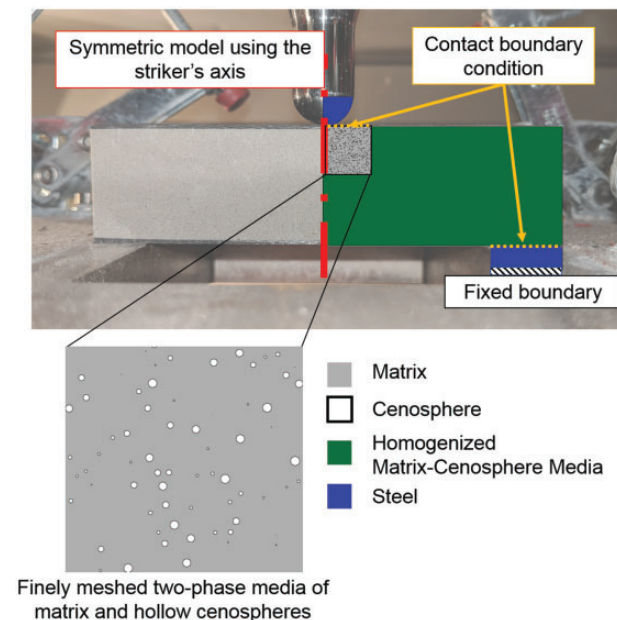


Figure 4. Domain of finite element model superposed on the experimental test setup. The enlarged square is the extent of the two phase media region. The vertical centerline restricts horizontal translation and enforces symmetric boundary condition.

Results and discussion

Internal damage through micro-CT scanning

Micro-CT scans of the impacted specimens were obtained using a Zeiss Metrotom 800 at the University of Wisconsin—Madison. The scans allowed

Table 2. Comparison between calculated homogenized foam modulus values using cenosphere modulus of 40 GPa and reported compressive modulus values for the syntactic foam core.

Cenosphere volume fraction	0%	20%	40%	60%
Reported modulus (GPa) ⁴²	3.4	3.9	4.7	4.8
Calculated modulus (GPa)	3.4	3.9	4.4	4.9
Reported strength (MPa) ⁴²	104.8	100.8	98.8	92.1

for the analysis of the damage mechanisms in the facesheets and crack propagation in the syntactic foam cores. Micro-CT images are shown in Figure 5, which are characteristic images corresponding to each cenosphere volume fraction and energy level. The rows of the table correspond to cenosphere volume fraction percentage, and the columns correspond to impact energy. A circular pattern is observed in the center of some of the images, which was a visual anomaly from the micro-CT process and not a physical characteristic of any specimen.

Figure 5(a) and (b) shows two specimens with 0% cenosphere volume fraction impacted at 80 J and 160 J each. For both energy levels, a majority of the damage occurred locally around the impact location with minimal damage in the core. For the 80 J specimen, a small indentation was observed in the facesheet which corresponded to matrix cracking. For the 160 J specimen, in addition to matrix cracking, fiber tearing and delamination between the facesheet and core were visible.

The 20% cenosphere volume fraction specimens exhibited a high degree of shear cracking that propagated through specimen thickness as shown in Figure 5(c) and (d). This is an undesirable failure mechanism as it typically leads to loss of structural integrity. On the other hand, localized crushing would be a less undesirable damage mechanism as the damage is contained in a localized region. At 80 J, shear cracks emanated conically outward from the impact location. Delamination from excessive deformation was also observed between the bottom facesheet and core. An additional damage mechanism was visible directly underneath the impact location which consisted of a slight discoloration of the core. This was attributed to localized compression of the core caused by the collapse of individual cenospheres and crushing of the surrounding matrix during impact. Similar damage mechanisms manifested at 160 J, but to a greater degree.

The micro-CT images for the 40% cenosphere volume fraction specimens are shown in Figure 5(e) and (f). Localized compression was observed under the impacted face at both 80 J and 160 J impact energies, while shear cracking manifested only in the 160 J case. The damage mechanisms for the 60% cenosphere volume fraction specimens were localized as compared to 20% and 40% cenosphere volume fraction

specimens and are shown in Figure 5(g) and 5(h). Under both impact energies, the 60% specimens exhibited localized compression in the foam core and fiber fracture in the top facesheet at the impact location. The localized damage in the 60% cenosphere volume fraction specimens was higher than any of the specimens tested. No shear cracking in the core or non-localized delamination between the core the facesheets was noticeable. The damage trend shown in the micro-CT images between specimens of different volume fractions translated into distinct mechanical responses from the impact tests, as discussed next.

Mechanical response from impact tests

The output data from each impact test were post-processed to determine their mechanical responses. Figure 6 shows characteristic force–displacement responses for the tests. Since the carbon fiber facesheets are stiffer than the foam core, the initial slope of the force–displacement plots is identical up to the point of initial penetration through the top facesheet. However, once the facesheets have been penetrated by the impact striker, the stiffness of the foam core is dominant, and the stiffness of the specimen is observed to decrease as the cenosphere volume fraction increases, regardless of the impact energy level. Based on the force–displacement responses, the initial stiffness ranged from 10–13 kN/mm for both the 80 J and 160 J tests. The peak contact force recorded for 160 J impact energy was higher than those corresponding to 80 J for all volume fractions of cenospheres. Moreover, for both impact energies, the peak force reduced with increasing cenosphere volume fraction. Sharp vertical drops in the post peak regime of the force–displacement responses were observed for specimens with cenosphere volume fractions of 20% and 40%. This corresponded to more damage in the specimens, which resulted in larger impact striker displacements and lower impact forces. The striker displacements and peak impact forces are summarized in Figure 7. An increase in striker displacement and a decrease in peak impact force were observed for the 20% cenosphere volume fraction specimens tested at 160 J. In addition, these specimens experienced the largest variation in test results as compared to the other volume fractions and impact energy levels.

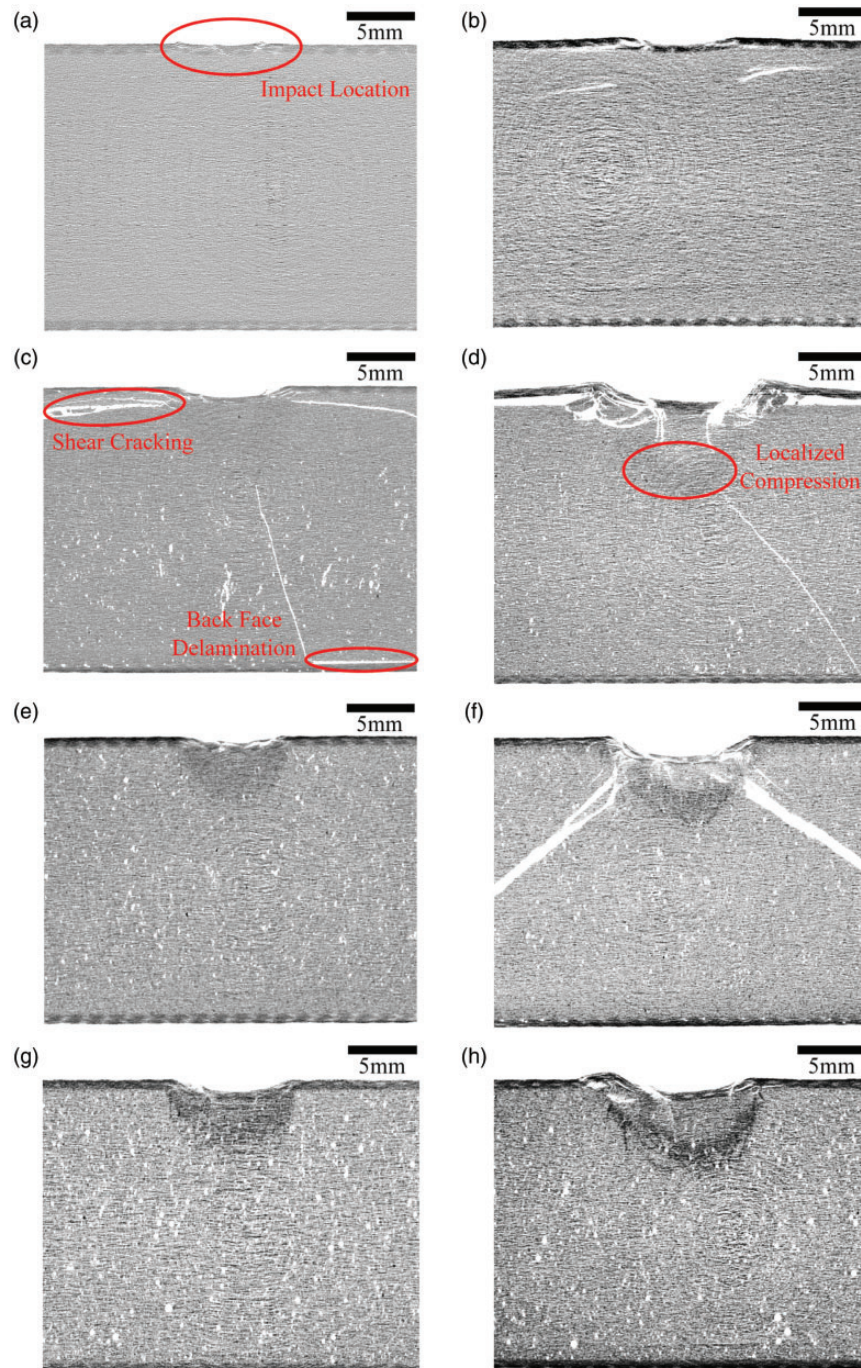


Figure 5. Typical micro-CT cross-sections for each cenosphere volume fraction and energy level tested. (a) 0% volume fraction 80 J, (b) 0% volume fraction 160 J, (c) 20% volume fraction 80 J, (d) 20% volume fraction 160 J, (e) 40% volume fraction 80 J, (f) 40% volume fraction 160 J, (g) 60% volume fraction 80 J, and (h) 60% volume fraction 160 J.

The summary plots shown in Figure 7 do not account for the decrease in density due to increased cenosphere volume fraction in the core. To account for the changing densities, summary plots showing the specific striker displacement and peak impact force are shown in Figure 8. These plots are very similar to those in Figure 7; however, the values were divided by

normalized weight ratios which change for specimens with different cenosphere volume fractions. The weight normalization, or in other words specific values, highlights the influence of weight reduction on the properties of the core. As a result, specific striker displacement and specific peak impact force both increased as the cenosphere volume fraction increased.

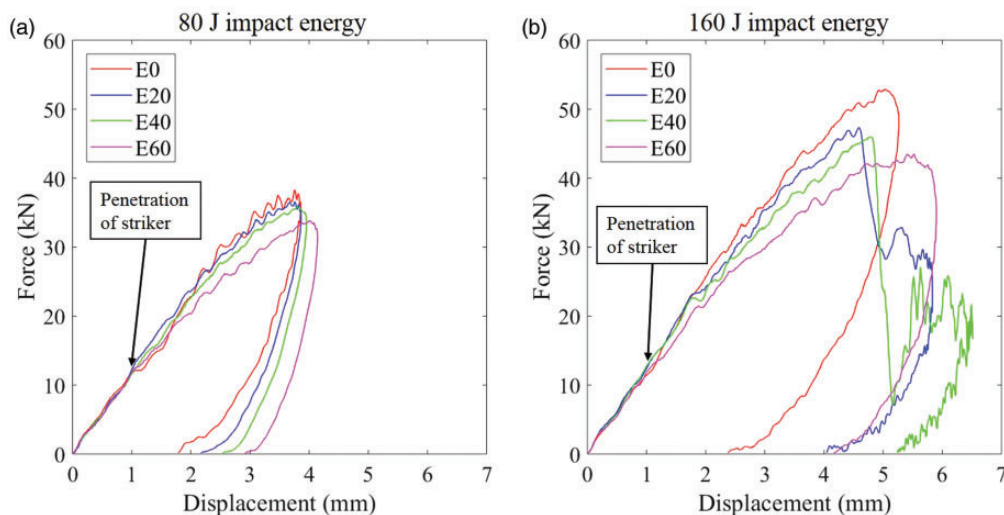


Figure 6. Force–displacement plots of impact specimens. (a) Specimens tested at 80 J and (b) specimens tested at 160 J.

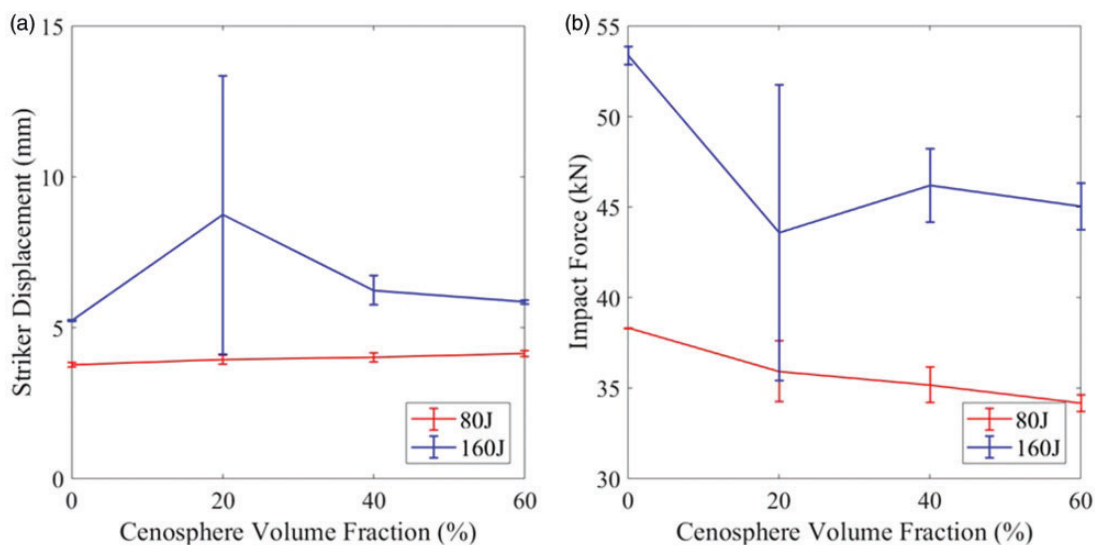


Figure 7. Summary plots of impact tests showing average values and standard deviation. (a) Striker displacement over the range of cenosphere volume fractions and (b) impact force over the range of cenosphere volume fractions.

Both the summary plots and micro-CT images have implied that the 20% specimens experienced the most damage and variation in peak impact force among all of the tested specimens. Further, the damage increased at the 160 J impact energy level. This is confirmed in Figure 9, which is a summary plot of the normalized absorbed energy for all the tests conducted. The absorbed energy is the amount of energy absorbed by the specimen upon impact by the striker, which is determined graphically from the energy versus time graph as depicted in Figure 9. To determine the normalized absorbed energy, the absorbed energy is divided by

the corresponding impact energy, which is the peak value in the energy versus time plot.

It is evident from the normalized absorbed energy plots in Figure 9 that 20% and 40% cenosphere volume fraction specimens were relatively more damaged than 0% and 60% specimens at 160 J impact energy as compared to 80 J. With that said, specimens with 0% and 60% cenosphere volume fractions experienced similar extent of damage at both energy levels of 80 J and 160 J. Higher apparent damage manifested by 20% and 40% cenosphere volume fraction specimens can be related to the shear cracking damage mechanism observed in

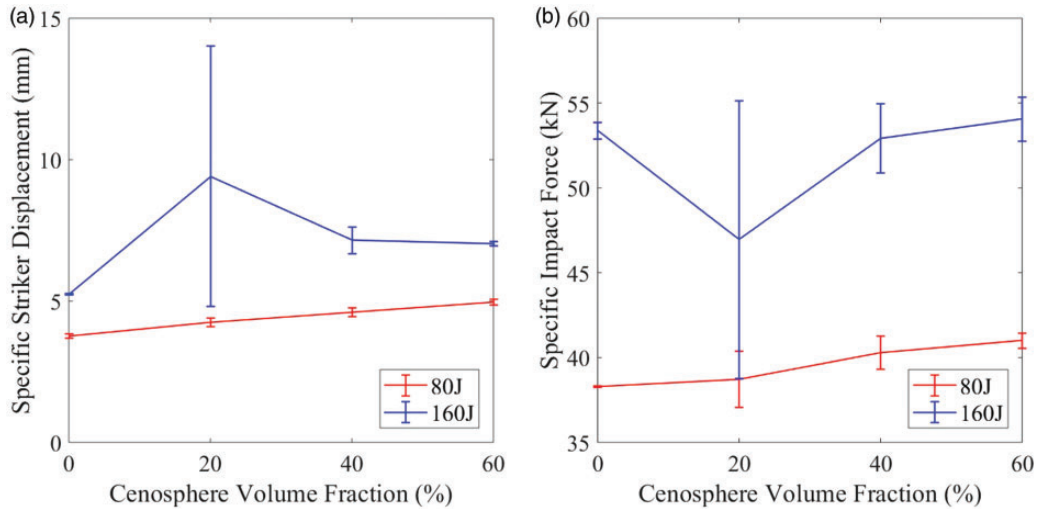


Figure 8. Summary plots of impact tests showing average values and standard deviation divided by a normalized ratio of specimen weight. (a) Striker displacement over the range of cenosphere volume fractions and (b) impact force over the range of cenosphere volume fractions.

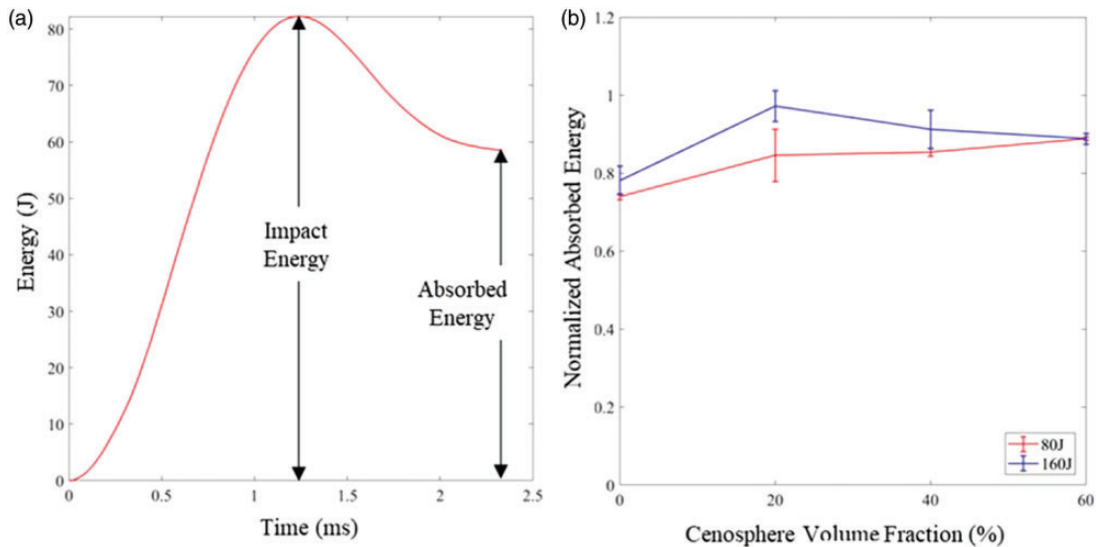


Figure 9. (a) Energy vs. time output for an arbitrary test specimen and (b) average normalized absorbed energy for all cenosphere volume fractions and energy levels.

these specimens as compared to the 60% volume fraction specimens that exhibited localized compression and absorbed similar levels of normalized energy at the two energy levels tested.

Damage mechanism observations and causes

The volume fraction of cenospheres in the syntactic foam cores influenced the damage mechanisms of the sandwich composites, especially under high impact energy of 160 J. This was more evident upon comparing the mechanical response results and micro-CT images.

Large shear cracks and delamination in the micro-CT scans corresponded to sharp vertical drops in the average maximum impact force recorded and correspondingly higher maximum striker displacements. Shear cracking, a highly undesirable failure mechanism as it typically leads to global failure, was observed in the core along with delamination between the core and the facesheets. This damage mechanism was most commonly observed in the 20% cenosphere volume fraction specimens tested under 160 J impact energy, but specimens with 20% cenosphere volume fraction tested at 80 J and specimens with 40% cenosphere volume

fraction tested at 160J also experienced shear cracking in few specimens. Localized compression (crushing) was the other common damage mechanism associated with the core and occurred directly underneath the impact striker and manifested itself in a discolored region in the micro-CT scan images.

From the damage mechanism observations, it can be concluded that the behavior of the sandwich composite is more favorable with higher cenosphere volume fraction in the syntactic foam core. That is, damage was more localized with increasing cenosphere volume fraction. An explanation for this observation stems from the behavior of the cenospheres in the syntactic foam. In the micro-CT images, it was observed that foam was crushed under the striker regardless of the energy level and cenosphere volume fraction. In samples with low cenosphere volume fraction, stress redistribution would cause a crack to propagate in the matrix between two cenospheres that are situated a distance from each other. On the other hand, as the cenosphere volume fraction increases, the cenospheres are situated close to each other. For the crack to propagate, it is hypothesized that it would either require crushing of more cenospheres or propagating cracks around additional cenospheres in a tortuous path prior to manifesting as large cracks in the core. This supports the observation of large shear cracks at 20% and 40% volume fractions samples, whereas local crushing in the 60% volume fraction samples.

Corroboration of damage mechanisms through computational modeling

The results of the FE analysis show the correlation between the cenosphere volume fraction and the level of damage underneath the impact striker. Matrix shear strain contour plots are shown in Figure 10 for models with 20%, 40% and 60% cenosphere volume fractions. The pure epoxy model was not included because it did

not exhibit stress concentrations within the core. These plots correspond to a striker displacement of 1.6 mm for each case. The purpose of this FE analysis was to compare the extent of localized strain underneath the striker, which is anticipated to correspond to the level of damage.

From the 60% cenosphere volume fraction model, it is observed that the areas of high strains are more dispersed and intermixed with areas with lower strain values. As a result, a web of cracks are more likely to form in these areas of closely packed cenospheres which helps promote the localized compression failure mechanism under the impact location. This localized web of cracks are expected to decrease as the cenosphere volume fraction decreases due to the larger distances between adjacent cenospheres. As the distance between cenospheres increases, failure mechanism with few large cracks is expected, which can be seen as a continuous region of high strain as depicted in the 20% cenosphere volume fraction model in Figure 10. Therefore, having a higher volume fraction of cenospheres is favorable as the cenospheres help dissipate the strain energy by either crushing or driving the crack around them, thereby, splitting large shear cracks into multiple smaller cracks. These smaller cracks are more localized and are constrained in the vicinity of the impact location, thereby containing the damage to a localized region.

Conclusion

Although there has been much effort to individually characterize both syntactic foams and sandwich composites under dynamic impact loading, there has been relatively little work to characterize and quantify the behavior of sandwich composites with syntactic foam cores under the same. In this study, sandwich composites with syntactic foam cores and varying cenosphere volume fractions were tested at two different impact energy levels to gain an understanding of their

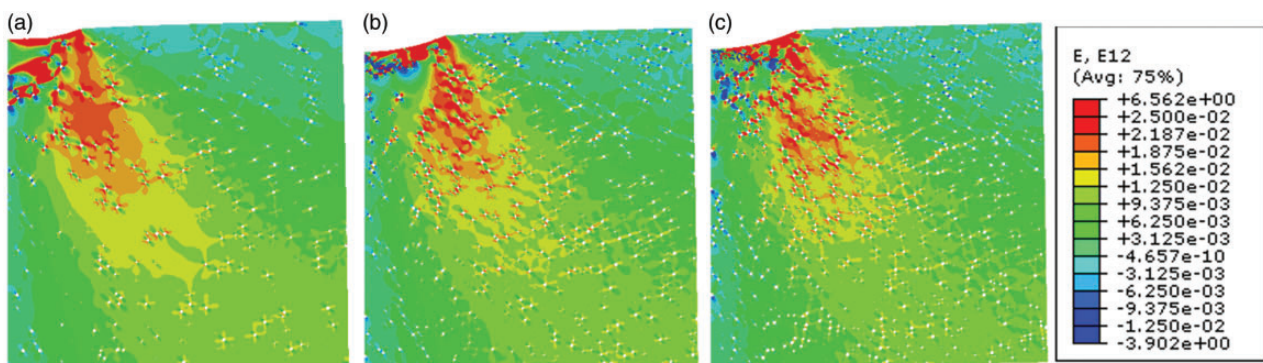


Figure 10. In-plane shear strain output of the two-phase media region shown in Figure 4 for the three different non-zero cenosphere volume fractions. (a) 20%, (b) 40%, and (c) 60%.

mechanical responses as well as the damage level and damage mechanisms. In addition, a FE model was developed to investigate the causes of the observed failure mechanisms.

Syntactic foam cores were fabricated with average cenosphere volume fractions of 0%, 20%, 40%, and 60% in epoxy. Then, sandwich composites were manufactured using VARTM process. For the facesheets, dry woven carbon fabric was used as reinforcement and vinyl ester resin as the matrix material. Impact tests on sandwich composites were conducted at two energy levels of 80J and 160J. The results of the impact tests showed a higher extent of damage and undesired damage mechanisms as the cenosphere volume fraction decreased for non-zero volume fraction cases (that is, 20%, 40%, and 60%). As observed from the micro-CT images, shear cracks within the syntactic foam core and face sheet damage were visible in the 20% and 40% cenosphere volume fraction specimens. In contrast, only localized compression underneath the impact location was observed in the 60% volume fraction specimens. An explanation for the observed undesired damage mechanisms in the 20% cenosphere volume fraction specimens was elucidated by developing a FE model. In the case with high cenosphere volume fraction, i.e. 60%, the strains redistributed around the cenospheres which led to a dispersed web of cracks that did not propagate the entire thickness of the syntactic foam core. For the models with lower cenosphere volume fractions, the distance between adjacent cenospheres was too large to form a web of cracks, and instead larger shear cracks were expected to form. In summary, this study showed that the syntactic foam cores with 60% cenospheres by volume are superior than other volume fractions investigated for the following reasons:

- The sandwich composites with 60% syntactic foams are less dense than the other specimens, being $\approx 18\%$ lighter than the pure epoxy core samples.
- Even though the initial stiffness of the 60% specimens was the most compliant of all specimens, it had comparable recorded average maximum impact force as compared to the other specimens with non-zero (that is, 20% and 40%) cenosphere volume fractions tested.
- The 60% volume fraction specimens experienced localized compression/crushing underneath the striker impact location at both energy levels. In contrast, other specimens with non-zero cenosphere volume fractions experienced at least some degree of shear cracking under high-energy impact loading. Localized compression/crushing as compared to shear cracks does not drastically affect the structural integrity of the core, whereas cascading effects such

as core/facesheet debonding are typically accompanied with large shear cracks in the core as seen in Figure 5. Hence, 60% volume fraction specimens are deemed to perform better compared to other cases considered in this study.

Although sandwich composites with high cenosphere volume fraction syntactic foams are shown to be desirable for containing impact damage, more studies need to be conducted by varying other properties like, core thickness, distribution of cenosphere dimensions (diameter and wall thickness), etc. before they can reliably be used in structural components subjected to dynamic impact loading.

Acknowledgements

The authors would like to thank Mechatronics Lab at UW-Madison for use of the micro-CT machine and also the Mechanical Engineering Department at the National Institute of Technology Karnataka (NITK), India for providing support and facilities for syntactic foam manufacturing.


Declaration of Conflicting Interests

The author(s) declared no potential conflicts of interest with respect to the research, authorship, and/or publication of this article.


Funding

The author(s) disclosed receipt of the following financial support for the research, authorship, and/or publication of this article: The authors would like to thank the U.S. Department of Defense (DoD) Office of Naval Research (ONR) Young Investigator Program (YIP) Grant [N00014-19-1-2206] through *Sea-based Aviation: Structures and Materials Program* for their partial support towards conducting the research presented here. The authors would also like to acknowledge the partial support from the U.S. DoD Defense Intelligence Agency (DIA) and ONR Solid Mechanics Program through the Basic Research Grant [W911NF-15-1-0430].

ORCID iDs

S Waddar  <https://orcid.org/0000-0002-0331-9637>

P Jeyaraj  <https://orcid.org/0000-0002-8456-8052>

P Prabhakar  <https://orcid.org/0000-0003-4654-1497>

References

1. Mouritz AP, Gellert E, Burchill P, et al. Review of advanced composite structures for naval ships and submarines. *Compos Struct* 2001; 53: 21–24.
2. Daniel IM, Gdoutos EE, Abot JL, et al. Deformation and failure of composite sandwich structures. *J Thermoplast Compos Mater* 2003; 16: 345–55.
3. Schubel PM, Luo JJ and Daniel IM. Low velocity impact behavior of composite sandwich panels. *Compos Part A: Appl Sci Manufac* 2005; 36: 1389–1396.

4. Zhang G, Wang B, Ma L, et al. Energy absorption and low velocity impact response of polyurethane foam filled pyramidal lattice core sandwich panels. *Compos Struct* 2014; 108: 304–310.
5. Wang J, Waas AM and Wang H. Experimental and numerical study on the low-velocity impact behavior of foam-core sandwich panels. *Compos Struct* 2013; 96: 298–311.
6. Nemes JA and Simmonds KE. Low-velocity impact response of foam-core sandwich composites. *J Compos Mater* 1992; 26: 500–519.
7. Mines RAW, Worrall CM and Gibson AG. Low velocity perforation behaviour of polymer composite sandwich panels. *Int J Impact Eng* 1998; 21: 855–879.
8. Erickson MD, Kallmeyer AR and Kellogg KG. Effect of temperature on the low-velocity impact behavior of composite sandwich panels. *J Sandw Struct Mater* 2005; 7: 245–264.
9. Salehi-Khojin A, Mahinfalah M, Bashirzadeh R, et al. Temperature effects on Kevlar/hybrid and carbon fiber composite sandwiches under impact loading. *Compos Struct* 2007; 78: 197–206.
10. Yang P, Shams SS, Slay A, et al. Evaluation of temperature effects on low velocity impact damage in composite sandwich panels with polymeric foam cores. *Compos Struct* 2015; 129: 213–223.
11. Tan KT, Watanabe N and Iwahori Y. X-ray radiography and micro-computed tomography examination of damage characteristics in stitched composites subjected to impact loading. *Compos Part B: Eng* 2011; 42: 874–884.
12. Hazizan MA and Cantwell WJ. The low velocity impact response of foam-based sandwich structures. *Compos Part B: Eng* 2002; 33: 193–204.
13. Elamin M, Li B and Tan KT. Impact damage of composite sandwich structures in arctic condition. *Compos Struct* 2018; 192: 422–433.
14. Gupta N and Woldesenbet E. Microballoon wall thickness effects on properties of syntactic foams. *J Cell Plast* 2004; 40: 461–480.
15. Gupta N, Woldesenbet E and Kishore. Compressive fracture features of syntactic foams-microscopic examination. *J Mater Sci* 2002; 37: 3199–3209.
16. Gladysz GM and Chawla KK. Syntactic and composite foams: proceedings of an engineering conferences international (eci) conference. *J Mater Sci* 2006; 41: 3959–3960.
17. Choqueuse D and Davies P. *Ageing of composites in underwater applications*. ISBN 9781845693527, 2008, pp.467–498.
18. Ambika Devi K, John B, Reghunadhan Nair CP, et al. Syntactic foam composites of epoxy-allyl phenol-bismaleimide ternary blend processing and properties. *J Appl Polym Sci* 2007; 105: 3715–3722.
19. Banhart J. Manufacture, characterisation and application of cellular metals and metal foams. *Prog Mater Sci* 2001; 46: 559–632.
20. Gupta N, Zeltmann SE, Shunmugasamy VC, et al. Applications of polymer matrix syntactic foams. *JOM* 2014; 66: 245–254.
21. Zhu B, Ma J, Wang J, et al. Thermal, dielectric and compressive properties of hollow glass microsphere filled epoxy-matrix composites. *J Reinf Plast Comp* 2012; 31: 1311–1326.
22. Yung K, Zhu B, Yue T, et al. Preparation and properties of hollow glass microsphere-filled epoxy-matrix composites. *Compos Sci Technol* 2009; 69: 260–264.
23. Jayavardhan M, Kumar BB, Doddamani M, et al. Development of glass microballoon/hdpe syntactic foams by compression molding. *Compos Part B: Eng* 2017; 130: 119–131.
24. Poveda RL, Dorogokupets G and Gupta N. Carbon nanofiber reinforced syntactic foams: degradation mechanism for long term moisture exposure and residual compressive properties. *Polym Degrad Stab* 2013; 98: 2041–2053.
25. Gupta N, Brar BS and Woldesenbet E. Effect of filler addition on the compressive and impact properties of glass fibre reinforced epoxy. *B Mater Sci* 2001; 24: 219–223.
26. Satapathy BK, Das A and Patnaik A. Ductile-to-brittle transition in cenosphere-filled polypropylene composites. *J Mater Sci* 2011; 46: 1963–1974.
27. Qiao J and Wu G. Tensile properties of fly ash/polyurea composites. *J Mater Sci* 2011; 46: 3935–3941.
28. Bharath Kumar BR, Doddamani M, Zeltmann SE, et al. Processing of cenosphere/HDPE syntactic foams using an industrial scale polymer injection molding machine. *Mater Des* 2016; 92: 414–423.
29. Kumar BR, Doddamani M, Zeltmann SE, et al. Data characterizing tensile behavior of cenosphere/HDPE syntactic foam. *Data Brief* 2016; 6: 933–941.
30. Barkoula NM, Alcock B, Cabrera NO, et al. Fatigue properties of highly oriented polypropylene tapes and all-polypropylene composites. *Polym Polym Compos* 2008; 16: 101–113.
31. Gupta N, Ye R and Porfiri M. Comparison of tensile and compressive characteristics of vinyl ester/glass microballoon syntactic foams. *Compos Part B: Eng* 2010; 41: 236–245.
32. Gladysz GM, Perry B, Meechen G, et al. Three-phase syntactic foams: structure-property relationships. *J Mater Sci* 2006; 41: 4085–4092.
33. Shunmugasamy VC, Pinisetty D and Gupta N. Viscoelastic properties of hollow glass particle filled vinyl ester matrix syntactic foams: effect of temperature and loading frequency. *J Mater Sci* 2013; 48: 1685–1701.
34. Gupta N, Woldesenbet E and Mensah P. Compression properties of syntactic foams: effect of cenosphere radius ratio and specimen aspect ratio. *Compos Part A: Appl Sci Manuf* 2004; 35: 103–111.
35. Maharsia R, Gupta N and Jerro HD. Investigation of flexural strength properties of rubber and nanoclay reinforced hybrid syntactic foams. *Mater Sci Eng A* 2006; 417: 249–258.
36. Tagliavia G, Porfiri M and Gupta N. Analysis of flexural properties of hollow-particle filled composites. *Compos Part B: Eng* 2010; 41: 86–93.
37. Tagliavia G, Porfiri M and Gupta N. Influence of moisture absorption on flexural properties of syntactic foams. *Compos Part B: Eng* 2012; 43: 115–123.

38. Kishore, Shankar R and Sankaran S. Short beam three point bend tests in syntactic foams. Part I: microscopic characterization of the failure zones. *J Appl Polym Sci* 2005; 98: 673–679.
39. Kishore, Shankar R and Sankaran S. Short-beam three-point bend tests in syntactic foams. Part II: effect of microballoons content on shear strength. *J Appl Polym Sci* 2005; 98: 680–686.
40. Kishore, Shankar R and Sankaran S. Short-beam three-point bend test study in syntactic foam. Part III: effects of interface modification on strength and fractographic features. *J Appl Polym Sci* 2005; 98: 687–693.
41. Garcia CD, Shahapurkar K, Doddamani M, et al. Effect of arctic environment on flexural behavior of fly ash cenosphere reinforced epoxy syntactic foams. *Compos Part B: Eng* 2018; 151: 265–273.
42. Shahapurkar K, Garcia CD, Doddamani M, et al. Compressive behavior of cenosphere/epoxy syntactic foams in arctic conditions. *Compos Part B: Eng* 2018; 135: 253–262.
43. Gupta N and Woldeesenbet E. Characterization of flexural properties of syntactic foam core sandwich composites and effect of density variation. *J Compos Mater* 2005; 39: 2197–2212.
44. ASTM. D7766-16 Standard practice for damage resistance testing of sandwich constructions. *ASTM* 2015; i: 1–9.